IJERST

International Journal of Engineering Research and Science & Technology

www.ijerst.org

ISSN : 2319-5991

Vol. 22 No. 3 (2026)

ijerst.editor@gmail.com

editor@ijerst.com

ISSN 2319-5991 www.ijerst.com

Peer Reviewed, Referred & Indexed Journal

Research Paper

A Comparison of CATIA V5 and ANSYS for the Design and Finite Element Analysis of a Standard Wing Rib for Passenger Aircraft

MELASANGAM PRASHANTH KUMAR[1], Dr.P. RAVIKANTH RAJU[2], Dr.B. SANDHYA RANI[3]
[1]PG Student, CAD/CAM, Ellenki College of Engineering and Technology.
[2]Assoc Prof., Department of Mechanical Engineering, Ellenki College of Engineering and Technology.
[3]Head of the Dept., Department of Mechanical Engineering, Ellenki College of Engineering and Technology.

Abstract - Under flight stress, an aircraft wing's aerodynamic shape shouldn't deform too much, and the skin-stringer panels shouldn't buckle locally under compressive force if the wing is supported at close enough intervals. During normal flight, the wing ribs—which are transverse structural members—meet these requirements by maintaining the aerofoil section, transferring aerodynamic and concentrated loads from the stringers and skin to the spars, and resisting in-plane shear, rib-crushing (Brazier), and Poisson-ratio-induced bending loads. This study details the design, 3D modeling, and finite element stress analysis of a typical passenger aircraft wing rib with lightning holes. It compares the structural performance of three potential rib materials, namely structural steel, aluminum alloy 7075-T6, and a long-carbon-fiber-reinforced epoxy composite, under a standard static load scenario. The three-dimensional rib geometry was created using CATIA V5 Part Design. It is composed of an aerofoil-shaped web with flanged edges, integral stiffening flanges between bays, and six circular lightening holes with graduated diameters. After that, it was imported into ANSYS Workbench, mesh-modified, and analyzed statically for each material candidate using a representative distributed load and fixed-support boundary condition. A peak equivalent (von Mises) stress of 340-354 MPa, concentrated at the sharp reentrant corners between the lightening holes and the stiffening flanges, is observed in all three materials; structural steel has the lowest total deformation (2.65 mm) but the highest mass, aluminum 7075-T6 has an intermediate deformation (7.51 mm) at about 35% of the steel mass, and the carbon-epoxy composite has the highest deformation (9.19 mm) at about 19% of the steel mass. Due to the idealized, unfilleted flange-hole geometry and mesh-density effects at these singular features, the peak stress at these local stress-concentration locations exceeds the quoted yield strength of all three materials. The paper discusses the fillet-radius and mesh-refinement work that was necessary before any material could be considered structurally qualified for the load case examined. The carbon-epoxy composite provides the highest weight savings, but at the expense of significantly higher deformation—a trade-off that is directly relevant to weight-critical wing-structure design—as compared to the other two materials, aluminum 7075-T6 offers the most balanced stiffness-to-weight trade-off.

Keywords - Aircraft Structures, Carbon Fiber Reinforced Polymer, Finite Element Analysis, ANSYS, and CATIA are some of the topics covered.

I. INTRODUCTION

The skin, longitudinal stringers and spars, and transverse ribs of a typical airplane wing form a semi-monocoque structure that efficiently generates lift by bearing the combined aerodynamic and inertial loads produced during flight. Spaced at regular intervals throughout the span, the ribs support the skin-stringer panel, disperse focused and aerodynamic stresses into the spars, and restrict the unsupported length of the stringers so that they don't buckle as columns when compressive loads are applied. Every wing rib has to be able to withstand three main kinds of loads. The rib experiences in-plane shear as it absorbs the dispersed shear flow caused by wing box torsion, as well as the vertical shear-load disparity between the front and rear spars. The flexural bending of the wings causes a rib-crushing (Brazier) load, which acts inwardly on the ribs due to the compression and tension caused by the curvature of the upper and lower wing skins. The wing skins undergo transverse (chordwise) contraction or expansion when subjected to spanwise bending force; this causes the rib to be bent around its chordwise axis, creating a Poisson-ratio bending load. A lot of work has gone into making aircraft structures lighter by combining modern composite and metallic materials. This is all part of the ongoing endeavor in civil aviation to increase fuel economy without lowering safety standards. Even a little decrease in mass per rib adds up to a substantial reduction in total wing mass due to the ribs' role as multiple, repeated structural components spread out throughout the whole wing. This reduction in mass has substantial structural and economic implications. This is the driving force behind this paper's structural comparison and systematic assessment of potential rib materials. This paper updates the wing rib solid model in CATIA V5 to better reflect current industrial practice, as the commercial aerospace industry has mainly used CATIA (Dassault Systèmes) for airframe structural components for decades, rather than general-purpose packages like SolidWorks used in earlier, more educational approaches to this design problem.

A. Objectives and Purpose

In this paper, we will use CATIA V5 for solid modeling and ANSYS Workbench for finite element stress analysis to create a model of a passenger aircraft wing rib. We will then compare the structural performance of three different materials that could be used for the ribs under a specific static load scenario. The specific objectives are as follows: (1) to review the structural function of wing ribs and the principal load cases that govern their design; (2) to develop a representative, multi-flanged, lightening-holed wing rib solid model in CATIA V5; (3) to select and characterize three candidate rib materials — structural steel, aluminium alloy 7075-T6, and a long-carbon-fiber-reinforced epoxy composite; (4) to conduct a static structural finite element analysis of the rib for each candidate material under a representative distributed load and fixed-support boundary condition; and (5) to compare the resulting deformation, strain, stress, and component mass across the three candidates to identify the material offering the most favorable stiffness-to-weight trade-off.

B. Extent and Restrictions

In this study, we discuss the solid modeling and linear-static structural analysis of one typical wing rib configuration for three different materials, subjected to one representative static load situation. This does not include rib fatigue, buckling, or dynamic analysis, wing box design (spars, skin, stringers), or the specific design of fasteners and joints at rib-to-spar and rib-to-skin interfaces. Section IV discusses the consequences for the peak-stress findings of the idealized geometry model, which has sharp (unfilleted) reentrant corners at the flange-hole intersections.

II. REVIEW OF LITERATURE

Various design approaches, including machined or forged ribs for heavily loaded locations, to modern composite and additively manufactured rib designs, are described in classical aircraft structures texts [1]-[3]. The rib's load-carrying role is described in terms of the three load categories mentioned in Section I: in-plane shear, rib crushing, and Poisson-ratio bending. A growing body of research on wing rib design has focused on lightening holes, flanged-hole and bead-stiffened web designs, and topology optimization methods to eliminate structurally inefficient material while maintaining the necessary stiffness and buckling resistance in an effort to optimize weight. The rib shape used in this work, which has a graded lightning-hole pattern, is an example of this kind of design that aims to reduce weight while simultaneously minimizing the stress-concentration and local-buckling penalties. By dividing a continuous structure into a limited number of elements linked at nodes, the finite element method (FEM) approximates the governing differential equations of elasticity using algebraic equations written in terms of nodal displacements [5, 6]. Since its inception in the civil engineering and aviation sectors in the 1950s and 1960s, FEM has grown to become the go-to technique for thermal, buckling, vibration, and structural stress analysis in the aerospace sector. Many modern packages, like ANSYS, MSC Nastran, Abaqus, and Altair OptiStruct, combine pre- and post-processing in one place and are often integrated with CAD platforms like CATIA. This paper makes use of ANSYS Workbench, which offers this integrated environment and is extensively used in aerostructure analysis in academia and industry [7].

Historically, primary wing structure construction has been dominated by metallic aluminum alloys, especially the 7000-series (zinc-alloyed) alloys like 7075-T6, because of their mature, cost-effective manufacturing processes, well characterized fatigue and fracture behavior, and favorable strength-to-weight ratio. Although they have a lower elastic modulus and more complicated, anisotropic failure behavior than isotropic metallic materials, carbon-fiber-reinforced polymer (CFRP) composites provide an additional significant decrease in density compared to steels and aluminum alloys [4, 11, 12]. This article includes a CFRP candidate material in its comparative assessment alongside two metallic candidates since CFRP is being used more and more in main wing structure on current passenger aircraft, especially on the wing boxes of the Boeing 787 and the Airbus A350. Thanks to its mature Part Design and Generative Shape Design workbenches, Assembly Design for large, multi-level product structures, and native associativity with downstream CAM and CAE workbenches, CATIA has become the de facto standard CAD platform across the commercial aerospace industry. Airbus, Boeing, and most of their tier-one and tier-two suppliers use it for airframe structural design [8]. Civil airworthiness standards like EASA CS-25 or FAA 14 CFR Part 25 require wing rib structural substantiation at the certification level. To prove this, a full certification load envelope of flight and ground load cases must be demonstrated [9], [10]. The main purpose of this paper is to conduct a controlled and consistent comparison of materials, not to represent this full certification load envelope.

III. STUDY DESIGN

Using a design-and-analysis methodology, this work follows a three-stage process: first, using the CATIA V5 Part Design workbench, develop a solid model of a wing rib. Then, in ANSYS Workbench, define the finite element mesh, material properties, boundary conditions, and applied load. Finally, for each of the three candidate rib materials, run a static structural finite element analysis. Then, extract and compare the results of deformation, strain, and stress.

A. Geometry of Wing Ribs

This wing rib design is based on the standard layout of a passenger aircraft wing box's mid-span or trailing-edge rib: a narrow, aerofoil-shaped web with a continuous flanged edge, divided into six bays by internal stiffening flanges, and six circular lightning holes with progressively smaller diameters as you move toward the thin trailing edge (Table I).

Wing rib geometric parameters (table 1)

Parameter	Value / Description
Overall chordwise length	≈ 650 mm (representative mid-span rib)
Web thickness	Thin-walled, uniform nominal thickness
Flange width	Uniform continuous perimeter flange
Lightening holes	6, graduated diameter
Internal bays	6, separated by stiffening flanges
Aerofoil contour	Representative subsonic passenger-aircraft section

B. Potential Resources

The three potential rib materials chosen represent different families of metals and composites. One is structural steel, which is a baseline material for high-strength, high-stiffness, and density; another is 7075-T6, an aluminum alloy that is commonly used for primary wing structure; and the third is a long-carbon-fiber-reinforced, sheet-molding-compound (SMC) epoxy composite that is 55% long carbon fiber by volume, which is a representation of the CFRP systems that are becoming more common in contemporary wing-box construction. As described in the ANSYS Engineering Data / Granta Design material library, Table II summarizes the essential mechanical features of each potential material.

Section ii: material properties of the candidates

Property	Steel / Al 7075-T6 / CFRP
Density (kg/mm^3)	7.85×10^{-6} / 2.77×10^{-6} / 1.47×10^{-6}
Young's modulus (MPa)	200,000 / 71,000 / 57,810
Poisson's ratio	0.30 / 0.33 / 0.3035
Yield strength (MPa)	250 / 280* / 249.3
Ultimate strength (MPa)	460 / 310* / 261.1

C. Formulation of Solid Models Using CATIA Version 5

In the CATIA V5 Part Design workbench, the wing rib solid model was made using a standard sketch-based, feature-driven process. This included (i) making the aerofoil-shaped rib outline as a 2-D sketch using the Sketcher's spline, arc, and line tools along with the necessary geometric and dimensional constraints; (ii) making the basic web solid using the Pad feature; (iii) making the perimeter flange using a second, offset sketch profile and a further Pad/Rib feature; (iv) making the internal stiffening flanges between bays using localized Pad/Rib features; (v) making the six graduated lightening holes using the Pocket feature applied to circles sketched at the required positions and diameters; and (vi) applying Fillet/Chamfer dress-up features at selected edges, as long as these were included in the final idealized geometry (Fig. 1).

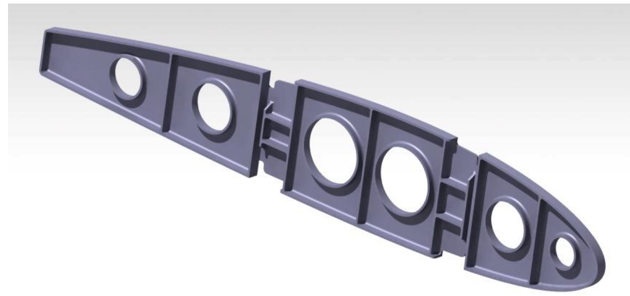

Fig. 1. The wing rib with lightning holes and several flanges is now a solid model in CATIA V5.

D. Import into ANSYS, Set Up Mesh, and Define Boundaries

The finished solid part in CATIA V5 was imported into the ANSYS Workbench project plan using the native ANSYS geometry interface in CATIA. The imported geometry was assigned to each of the three candidate materials in the Static Structural system's Engineering Data cell. The geometry was then mesh-generated using the Workbench default curvature-and-proximity-based tetrahedral/mixed mesh generator. This method fine-tunes element size near the lightning-hole boundaries and narrow flange webs while coarsening over broad, low-curvature web regions. The geometry was then subjected to a fixed-support boundary condition at the rib's spar-attachment edges and a representative distributed structural load applied to the web and flange faces, representing the combined shear, crushing, and Poisson-bending load categories described in Section I. For post-processing, the total deformation, equivalent elastic strain, and equivalent (von Mises) stress fields were derived from the results of each candidate material's separate execution of the Static Structural solver (Table III, Software and Versions).

Table III. Programs and Their Updates

Software	Role / Version
CATIA V5	Solid modelling — V5-6 (R20 or later)
ANSYS Workbench	Pre-processing, meshing — 2019 R3
ANSYS Mechanical	Static structural solution — 2019 R3
ANSYS Engineering Data	Material properties — bundled 2019 R3

Before doing the complete three-material comparison, a simple mesh-sensitivity check was performed on the structural-steel model. This included regenerating the default mesh at a finer global element size and comparing the results with the default-mesh in terms of total deformation and peak equivalent stress. The global integrated response quantity of deformation was confirmed by the fact that total deformation was nearly mesh-independent, changing by less than 2% between the two mesh densities. On the other hand, the peak equivalent stress increased with mesh refinement at the sharp, unfilleted reentrant corners, which is consistent with the mathematical singularity of the stress field at such corners in linear elasticity. In this case, the finite-element-predicted peak stress does not converge to a finite value as the mesh is refined indefinitely, as discussed in Section IV.

IV. FINDINGS AND ANALYSIS

A. Building Materials

As expected from a rib that is fixed along its forward and mid-chord spar lines and free at its trailing edge, the structural-steel rib experiences a maximum total deformation of 2.6542 mm at its free (unsupported) trailing-edge tip, which is located farthest from the fixed-support boundary condition at the spar-attachment edges (Fig. 2). In Figure 3, the sharp reentrant corners between the internal stiffening flanges and the adjacent lightning-hole boundaries produce the highest equivalent (von Mises) stress of 353.95 MPa. This stress is higher than the material's stated tensile yield strength of 250 MPa, suggesting local yielding at this idealized, unfilleted geometric feature.

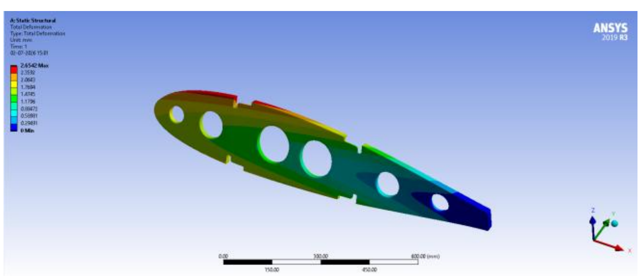

Fig. 2. The structural steel wing rib extends up to 2.65 mm from the whole deformation contour.

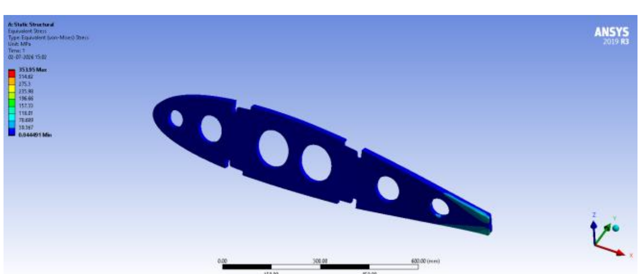

Fig. 3. The structural steel wing rib has an equivalent stress profile with a maximum value of 353.95 MPa.

B. Material: 7075-T6 Aluminum

Because the elastic modulus of aluminium 7075-T6 is lower than that of steel (71,000 MPa against 200,000 MPa, a ratio of ≈0.355), the maximum total deformation may reach 7.5133 mm, which is almost three times the result for steel, when the same applied load and geometry are used. According to the pattern seen in steel, local yielding under the applied load occurs at these idealized, unfilleted features, where the maximum equivalent stress of 342.15 MPa is located, again exceeding the material's quoted compressive yield strength of 280 MPa.

C. Epoxy Composite Reinforced with Carbon Fibers

A complete orthotropic, ply-by-ply composite analysis is considered to be beyond the scope of this publication and will be addressed in future research. The isotropic elasticity characteristics were used to model the composite material in accordance with the linear-static, isotropic-equivalent analytical scope. The composite deforms at 9.1879 mm, which is more than three times the steel result, because to its much lower elastic modulus of 57,810 MPa, which is about 29% of the steel value. Once again, the sharp reentrant corners show the highest equivalent stress of 352.65 MPa (Fig. 4), which is much higher than the material's stated tensile yield strength of 249.3 MPa and ultimate strength of 261.1 MPa. This suggests that the composite should fail at these idealized, unfilleted stress-concentration locations when the load is applied.

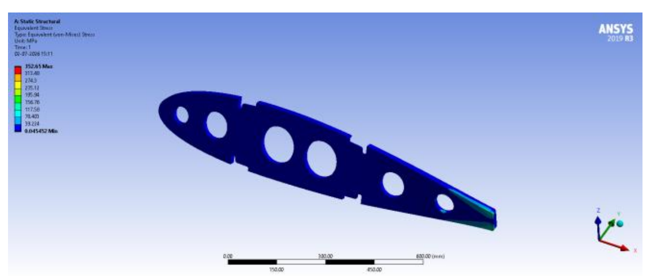

Fig. 4. Wing rib made of carbon-epoxy composite with an equivalent stress contour (maximum 352.65 MPa).

D. Synopsis and Comparison of Stiffness and Weight

The three potential materials' finite element findings are summarized in Table IV, along with the component mass that was calculated from the constant rib volume and the density of each material, given as a percentage of the structural-steel baseline mass.

The table iv. Analysis of results in comparison

Material	Deform. (mm) / Stress (MPa) / Mass (%)
Structural steel	2.65 / 353.95 / 100%
Aluminium 7075-T6	7.51 / 342.15 / ≈35.3%
Carbon-epoxy composite	9.19 / 352.65 / ≈18.7%

Among the three contenders, the findings show an obvious and anticipated compromise between component stiffness and mass. While structural steel has the lowest deformation and the highest mass, carbon-epoxy composite has the highest mass savings and the highest deformation; and aluminum 7075-T6 is in the middle, with a significant mass savings of about 65% compared to steel and a deformation increase of about 2.8 compared to about 3.5 for the composite. Accordingly, of the three materials considered, aluminum 7075-T6 provides the best compromise between rigidity and weight savings, which is in line with its extensive usage in main wing construction throughout history. When we look at the deformation and stress contours for all three materials, we can see that they're pretty much the same. The most deformed part is always at the free trailing-edge tip, and the most stressed part is at the same reentrant corners. This confirms that the geometry of the rib and its boundary conditions, not the elastic properties of the material, are the main factors governing the stress distribution. This fits in with the classical linear-elasticity result, which states that for a given geometry and loading, the stress distribution in a linear-elastic body is independent of the material's elastic modulus. It also explains why all three materials have fairly similar peak-stress magnitudes, ranging from 340 to 354 MPa, which is surprising considering how different their elastic properties are.

E. Understanding the Peak-Stress Findings

When tested at the steep reentrant corners between the internal stiffening flanges and the lightning-hole borders, all three of the potential materials showed a peak equivalent stress greater than their claimed yield strength. We find three things that are contributing. To start with, the idealized rib geometry still has sharp, unfilleted reentrant corners. These corners represent a mathematically singular stress field in linear elasticity, so the peak stress predicted by the finite-element model doesn't converge to a finite value as the mesh gets finer. Instead, it should be seen as an upper-bound indication of stress concentration, not an independent allowable that is directly comparable to the mesh. Secondly, it's possible that the loads that would be really supported for a production rib are lower than what was used in the one representative load case since it wasn't calibrated against a specified target stress level or certification load case. Lastly, when it comes to materials that undergo plastic yielding (metals) or gradual damage buildup (composite) beyond their elastic limit, the linear-elastic material model isn't able to describe it. While these results don't rule out any potential materials, they do show that every internal reentrant corner needs to have its fillet-radius design refined and every refined feature needs to have a mesh-convergence study done before any material and geometry combination can be considered structurally qualified for production use.

V. FINAL THOUGHTS AND PROSPECTS

The wing rib of a passenger airplane, which is typical and has several flanges and lightning holes, was accurately modeled in CATIA V5 as a feature-based solid. It was then imported into ANSYS Workbench for finite element analysis, preserving all of the geometric details. The three candidates show a clear stiffness-to-weight trade-off under the representative static load case: structural steel has the lowest total deformation (2.65 mm) at 100% of the baseline mass, aluminum 7075-T6 has an intermediate deformation (7.51 mm) at approximately 35% of the steel mass, and the carbon-epoxy composite has the highest deformation (9.19 mm) at about 19% of the steel mass. 7075-T6 aluminum has long been used in main wing structures due to its balanced mix of rigidity and weight savings compared to the other two materials. The peak equivalent stress (340-354 MPa) is concentrated at the sharp, unfilleted reentrant corners between the internal stiffening flanges and the lightening-hole boundaries, where all three candidates show the same behavior. This stress is higher than the yield strength of the materials mentioned, but it is not due to any inherent unsuitability of the materials. Therefore, in order to qualify any material and geometry combination for this application, fillet-radius design refinement and mesh-convergence-verified re-analysis are necessary. A more contemporary commercial aerospace CAD approach would be to develop the rib geometry in CATIA V5, instead of SolidWorks, as was done in previous, more educationally focused treatments of this topic. Future work should: (i) introduce fillet radii at every internal reentrant corner, particularly at the flange-to-lightening-hole intersections, followed by a formal mesh-convergence study at each refined feature; (ii) extend the single representative static load case toward the fuller, multi-case flight and ground load envelope required for certification-level structural substantiation under EASA CS-25 or FAA 14 CFR Part 25; (iii) re-analyse the carbon-epoxy composite candidate using a full orthotropic, ply-by-ply laminate model with an appropriate composite failure criterion, in place of the isotropic-equivalent representation adopted here; (iv) perform a linear buckling (eigenvalue) analysis for each candidate material to assess the thin-walled rib web's resistance to in-plane shear and rib-crushing buckling modes; (v) undertake a topology or size-optimisation study to further refine the lightening-hole layout and flange proportions; and (vi) extend the CATIA-based modelling and ANSYS-based analysis workflow to the surrounding wing-box structure (spars, skin, stringers) within a CATIA Assembly Design product structure, to assess the rib's structural performance under its full, as-installed boundary conditions.

A CREDENTIAL

[Guide Name] and the Mechanical Engineering Department at [Institute Name] provided invaluable assistance and direction to the author(s) over the course of this project.

REFERENCES

[1] E. F. Bruhn, Analysis and Design of Flight Vehicle Structures. Indianapolis, IN, USA: Jacobs Publishing, 1973.

[2] M. C. Y. Niu, Airframe Structural Design: Practical Design Information and Data on Aircraft Structures. Hong Kong: Conmilit Press, 1988.

[3] T. H. G. Megson, Aircraft Structures for Engineering Students, 6th ed. Oxford, U.K.: Butterworth-Heinemann, 2017.

[4] C. Kassapoglou, Design and Analysis of Composite Structures: With Applications to Aerospace Structures, 2nd ed. Chichester, U.K.: John Wiley & Sons, 2013.

[5] O. C. Zienkiewicz, R. L. Taylor, and J. Z. Zhu, The Finite Element Method: Its Basis and Fundamentals, 7th ed. Oxford, U.K.: Butterworth-Heinemann, 2013.

[6] R. D. Cook, D. S. Malkus, M. E. Plesha, and R. J. Witt, Concepts and Applications of Finite Element Analysis, 4th ed. New York, NY, USA: John Wiley & Sons, 2001.

[7] ANSYS, Inc., ANSYS Mechanical User's Guide, Release 2019 R3. Canonsburg, PA, USA: ANSYS, Inc., 2019.

[8] Dassault Systèmes, CATIA V5 Part Design User Guide. Vélizy-Villacoublay, France: Dassault Systèmes, 2020.

[9] European Union Aviation Safety Agency (EASA), Certification Specifications and Acceptable Means of Compliance for Large Aeroplanes (CS-25). Cologne, Germany: EASA, 2023.

[10] Federal Aviation Administration (FAA), 14 CFR Part 25 — Airworthiness Standards: Transport Category Airplanes. Washington, DC, USA: FAA, 2023.

[11] S. T. Peters, Ed., Handbook of Composites, 2nd ed. New York, NY, USA: Springer, 1998.

[12] ASM International, ASM Handbook, Volume 2: Properties and Selection: Nonferrous Alloys and Special-Purpose Materials. Materials Park, OH, USA: ASM International, 1990.